ROADWAY SAFETY INSTITUTE

Human-centered solutions to advanced roadway safety

A Novel Collision Avoidance System for a Bicycle

Woongsun Jeon
Rajesh Rajamani

Department of Mechanical Engineering
University of Minnesota

Final Report

REGION 5

CTS 18-06

University of Minnesota Driven to Discover
The University of Akron
Illinois University of Illinois at Urbana-Champaign
Southern Illinois University Edwardsville
Western Michigan University

Technical Report Documentation Page

1. Report No. CTS 18-06	2.	3. Recipients Accession No.
4. Title and Subtitle A Novel Collision Avoidance System for a Bicycle		5. Report Date April 2018 6.
7. Author(s) Woongsun Jeon, Rajesh Rajamani		8. Performing Organization Report No.
9. Performing Organization Name and Address Department of Mechanical Engineering University of Minnesota 111 Church Street SE Minneapolis, MN 55455		10. Project/Task/Work Unit No. CTS #2015020 11. Contract (C) or Grant (G) No. DTRT13-G-UTC35
12. Sponsoring Organization Name and Address Roadway Safety Institute Center for Transportation Studies University of Minnesota 200 Transportation and Safety Building 511 Washington Ave. SE Minneapolis, MN 55455		13. Type of Report and Period Covered Final Report 14. Sponsoring Agency Code
15. Supplementary Notes http://www.roadwaysafety.umn.edu/publications/		

16. Abstract (Limit: 250 words)

This project focuses on development of a sensing and estimation system for a bicycle to accurately detect and track vehicles for two types of car-bicycle collisions. The two types of collisions considered are collisions from rear vehicles and collisions from right-turning vehicles at a traffic intersection. The collision detection system on a bicycle is required to be inexpensive, small and lightweight. Sensors that meet these constraints are utilized.To monitor side vehicles and detect danger from a right-turning car, a custom sonar sensor is developed. It consists of one ultrasonic transmitter and two receivers from which both the lateral distance and the orientation of the car can be obtained. A Kalman Filter-based vehicle tracking system that utilizes this custom sonar sensor is developed and implemented. Experimental results show that it can reliably differentiate between straight driving and turning cars. A warning can be provided in time to prevent a collision. For tracking rear vehicles, an inexpensive single-beam laser sensor is mounted on a rotationally controlled platform. The rotational orientation of the laser sensor needs to be actively controlled in real-time in order to continue to focus on a rear vehicle, as the vehicle's lateral and longitudinal distances change. This tracking problem requires controlling the real-time angular position of the laser sensor without knowing the future trajectory of the vehicle. The challenge is addressed using a novel receding horizon framework for active control and an interacting multiple model framework for estimation. The features and benefits of this active sensing system are illustrated first using simulation results. Then, extensive experimental results are presented using an instrumented bicycle to show the performance of the system in detecting and tracking rear vehicles during both straight and turning maneuvers.

17. Document Analysis/Descriptors Bicycle crashes, Safety, Crash avoidance systems, Tracking systems, Sensors, Active safety systems		18. Availability Statement No restrictions. Document available from: National Technical Information Services, Alexandria, Virginia 22312	
19. Security Class (this report) Unclassified	20. Security Class (this page) Unclassified	21. No. of Pages 43	22. Price

A NOVEL COLLISION AVOIDANCE SYSTEM FOR A BICYCLE

FINAL REPORT

Prepared by:

Woongsun Jeon
Rajesh Rajamani
Department of Mechanical Engineering
University of Minnesota

April 2018

Published by:

Roadway Safety Institute
Center for Transportation Studies
University of Minnesota
200 Transportation and Safety Building
511 Washington Ave. SE
Minneapolis, MN 55455

ACKNOWLEDGMENTS

The funding for this project was provided by the United States Department of Transportation's Office of the Assistant Secretary for Research and Technology for the Roadway Safety Institute, the University Transportation Center for USDOT Region 5 under the Moving Ahead for Progress in the 21st Century Act (MAP-21) federal transportation bill passed in 2012.

TABLE OF CONTENTS

LIST OF FIGURES

LIST OF TABLES

EXECUTIVE SUMMARY

Approximately 49,000 bicyclist-motorist crashes and over 700 bicyclist fatalities occur each year in the US. This project focuses on development of a sensing and estimation system for a bicycle to accurately detect and track vehicles for two types of car-bicycle collisions. The two types of collisions considered are collisions from rear vehicles and collisions from right-turning vehicles at a traffic intersection. While approximately 40% of bicycle-car collisions are estimated to be from rear vehicles, one study estimates right-turning vehicles to be involved in 16% of motorist-bicyclist collisions. Thus, both the types of collisions studied in this project are of significant importance. When a potential collision is predicted by the vehicle tracking system on the bicycle, a loud horn is used to alert the motorist to the presence of the bicycle.

The collision avoidance system and vehicle tracking sensors used on cars cannot directly be re-utilized on bicycles. A typical radar used on a car can cost several thousand dollars and would be too large for use as a bicycle accessory. This project requires the total retail cost of all components used by the collision detection system on the bicycle to be less than $500. While the collision detection system on a bicycle is required to be inexpensive, small and lightweight, it must track a different and larger set of vehicle maneuvers compared to a forward collision avoidance system on a car. For example, a bicycle must account for side and rear collisions.

To monitor side vehicles and detect danger from a right-turning car, a custom sonar sensor is developed. It consists of one ultrasonic transmitter and two receivers (with a total cost below $20) from which both the lateral distance and the orientation of the car can be obtained. A Kalman Filter based vehicle tracking system that utilizes this custom sonar sensor is developed and implemented on the bicycle. Experimental results show that it can reliably differentiate between straight driving and right turning cars, so that a potential collision can be differentiated from a passing vehicle. A warning can be provided in time to prevent a collision.

For tracking rear vehicles, an inexpensive single-beam laser sensor is mounted on a rotationally controlled platform. While the laser sensor is inexpensive (cost $89), it has a single thin beam that provides only one distance measurement in the direction where it is oriented. Rotational scanning of the rear with the laser sensor is too slow for reliable collision prevention, since it provides only occasional distance updates on the rear vehicle. The rotational orientation of the laser sensor therefore needs to be actively controlled in real-time in order to continue to focus on a rear vehicle, once the presence of a rear vehicle has been detected. As the vehicle's lateral and longitudinal distances change, the orientation of the laser sensor needs to change. This tracking problem requires controlling the real-time angular position of the laser sensor without knowing the future trajectory of the vehicle. The challenge is addressed using a novel receding horizon framework for active control and an interacting multiple model framework for estimation of the vehicle's trajectory. The features and benefits of this active sensing system are illustrated first using simulation results. Then, extensive experimental results are presented using an instrumented bicycle to show the performance of the system in detecting and tracking rear vehicles during both straight and turning maneuvers of the rear vehicle.

Finally, data on real-world performance of the rear collision prevention system is obtained by conducting tests on a regular urban road near the University of Minnesota. The developed system is found to work reliably and to track all rear vehicles within the designed domain of interest.

Future work that would enhance the collision detection system and enable implementation of this research are identified. These include the development of a sensor fusion system that combines the use of the side sonar and the rear collision laser sensor, the conducting of a rigorous field operational test, the development of visual and audio warning systems that are human-centered and effective, and the development of a vehicle tracking system for addressing collisions from cross-traffic and left turning vehicles at a traffic intersection. These tasks are planned to be taken up in a new research project for which the PI (together with other collaborators) has received NSF funding.

A number of videos that show the performance of the developed collision prevention system during scenarios involving various rear vehicle maneuvers and various right-turning vehicle maneuvers have been made available on the internet for public viewing. These videos can be found at the following web site: **http://www.me.umn.edu/~rajamani/download/BicycleVideos/**

CHAPTER 1: INTRODUCTION

Over 49,000 bicyclist-motorist crashes were reported to police and resulted in 726 bicyclist fatalities in the US in 2012 [1]. Likewise, a recent report from the Insurance Institute for Highway Safety (IIHS) finds that more than 3,300 bicyclist fatalities occurred in a five-year period from 2008 to 2012 [2]. In the IIHS study, 45% of the fatalities involved a vehicle traveling in the same direction as a bicyclist [2]. This implies that the most common fatal bicyclist-motorist crash is likely by a vehicle approaching from behind the bicycle. Another report from the League of American Bicyclists [3] also finds that the most common bicyclist-motorist collision type is a rear end collision (40%) which is "a hit from behind". Additionally, a sideswipe collision (4%) is also caused by a vehicle initially approaching from the rear [3]. A report on bicycle accidents that occurred between 2001 to 2010 in Minneapolis [4] documented that the most common pre-crash maneuvers for motorists are vehicle following roadway (42%), vehicle making left turn (18%) and vehicle making right turn (16.4%).

This project addressed collisions due to rear vehicles and right-turning vehicles at a traffic intersection. The collision prevention system can be used to predict impending collisions and provide warnings to both the bicyclist and the involved motorist. Since a majority of these crashes are due to motorist being inattentive or careless [3, 4], the collision warning system will focus on warning the motorist. If a danger of collision is detected, the bicycle could provide a visual alert, followed by a more intrusive increasingly intensive audio signal if the visual alert is inadequete. Having a sensor system entirely on a bicycle provides safety enhancement without a requirement for all the vehicles on the road to be instrumented with bicycle detection sensors.

Automotive companies have developed a number of forward collision avoidance systems. Many of these systems utilize LIDAR or radar sensors or a combination of these [5-9]. However, these sensors are too big and too expensive (typically costing thousands of dollars) for a bicycle.

Aftermarket camera-based collision avoidance systems such as Mobileye [12] have also been commercially developed for cars. However, a continuous camera-based system is difficult to power using batteries on a bicycle. Further, such a camera-based system has a hardware cost of over $850 and additionally requires professional installation ($150) [12].

Another avenue of research has been the use of aftermarket camera systems on cars and buses to detect bicycles and pedestrians [10, 11]. Bicyclists cannot depend on all the cars on the road being instrumented with such bicycle detection systems for their safety. It is likely to take decades before such systems can achieve adequate penetration among all vehicles on the road to make bicycling safer.

As opposed to automotive research, very little research resources are currently spent on improving technology for bicycle safety. To the best of this research team's knowledge, sensor systems for bicycles have been explored only by a few research teams [13 - 16] and just two companies [17, 18]. The sensor systems currently explored for bicycles are limited in that the sensor systems are unable to provide vehicle maneuver information to bicyclists and do not provide real-time warnings to the involved motorists. The current sensor systems that have been explored in literature for a bicycle are summarized in Table I.

Table 1. Current Sensor Systems Explored for a Bicycle

Sensor Type	Specific Sensor	Description
Sonar [13], [18]	MaxBotix MB1202	• Low cost and low power consumption • Limited sensing range (less than 10m) • Does not provide target vehicle maneuver (passing versus right behind)
Radar [17]	Garmin Varia	• Long sensing range (up to 140m) • Dose not provide target vehicle maneuver (passing versus right behind)
Magnetometer [14], [15]	Honeywell HMC1052L	• Good performance for close proximity and for most environmental conditions • Limited sensing range (2m) • Does not provide target vehicle maneuver (passing versus right behind)
Optical (camera) [16]	Sony Handicam DCR-SX40	• Very detailed information • Limits in weather and lighting conditions • Computationally expensive

Figure 1 shows the two types of car-bicycle crashes that will be addressed in this project, namely collisions from rear vehicles and collisions from right turning vehicles at a traffic intersection.

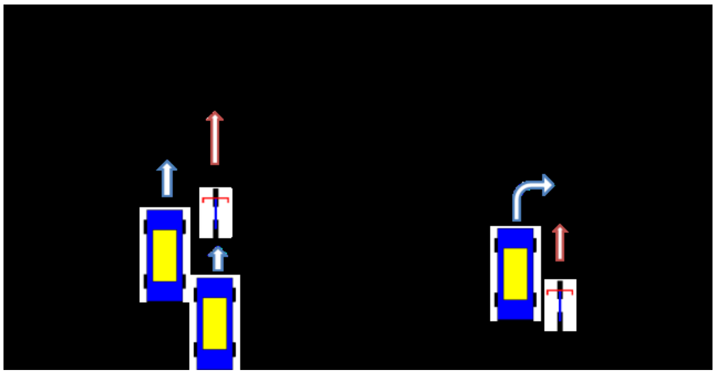

Figure 1. Two types of crashes at intersection addressed in this project

CHAPTER 2: SIDE COLLISION WARNING SYSTEM

When a bicycle is in the blind spot of a driver, the bicyclist could be in danger due to a right turning car, as shown in Figure 2. In order to prevent a collision, a sensor system that can detect and track the car during this maneuver is needed. A custom-designed sonar sensor system is developed on the left side of the bicycle to address this scenario.

2.1 CHALLENGES WITH SIDE COLLISION WARNING SYSTEM

Bicyclist-motorist crashes in which the bicycle is riding through the intersection while the motorist is making a right turn have relatively small pre-collision space and occur very quickly. Thus, a rapid warning decision is necessary. Also, the warning system needs to provide an alert to the motorist in order to make the motorist aware of the bicyclist's presence. Typically the motorist fails to see the bicyclist in this type of collision although the motorist has more control to avoid or mitigate damage from the collision. Another challenge in this collision warning scenario is that the warning system needs to predict the right turning car maneuver in sufficient time for the warning to be effective. Since response time is estimated to be 0.8 seconds for a human driver, the warning needs to be provided more than 1 second before predicted collision for it to be useful. Further, unnecessary loud warnings will cause sound pollution on the roads and unnecessary distraction to motorists. Hence, the collision prediction system needs to perform accurately with low false alarm rates. Thus, the warning system needs to detect the right turning car both accurately and promptly.

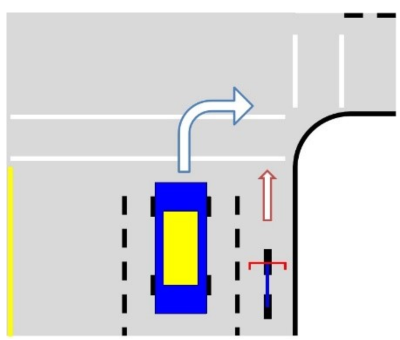

Figure 2. Side collision by a right turning vehicle.

Sonar sensors are considered for this system since they have suitable price, weight and size for a bicycle application. However, there is a difficulty in early prediction of the side car's maneuvers and in differentiating between a straight driving and turning car. Figure 3 shows that early sensor measurements are similar in both of these cases. Due to sonar sensor characteristics and common car shapes, the range measurement from the sensor decreases when the side car is entering the sensing region of the sonar. After the car fully enters in the sensing region, the two maneuver cases then provide different trends of the range measurement. However, it is too difficult to predict the turning maneuver early using only range measurement information. Consequentially, more information is needed and a custom sonar sensor that can measure both range and vehicle orientation is developed in section *B.* More details will also be provided using experimental data in section *C*, on distinguishing between the two maneuvers.

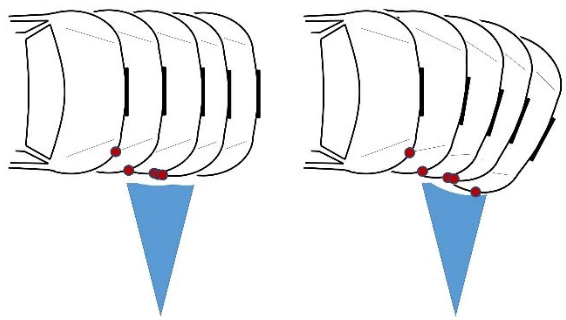

Figure 3. Similar measurement pattern (Red dot) from two different maneuvers when a car enters the sensing region (Blue region).

2.2 CUSTOM-DESIGNED SONAR SENSOR SYSTEM

Figure 4. Instrumented bicycle.

Figure 4 shows the proposed sonar sensor system on a bicycle. The sensor system is composed of one transmitter and two receivers so that it can measure not only the distance to the object, but also the angular orientation of the object's side surface. This system can be operated with a 50Hz sampling rate and provides up to a 6m range measurement.

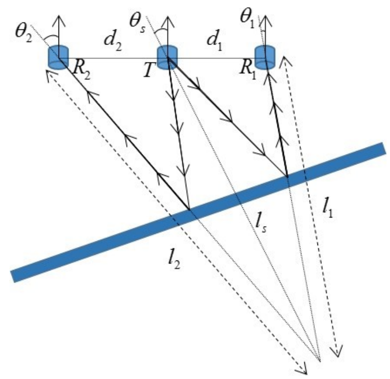

Figure 5. Sonar system with one transmitter and two receivers [26].

The schematic in Figure 5 describes the construction and operation of the custom sonar system. A sound wave is initiated from the transmitter T and the echoes are detected by the two receivers R_1 and R_2 located at longitudinal distances d_1 and d_2 from the transmitter as shown in Figure 5. Measuring the time that sound takes to travel from the transmitter to the receivers, the travel distance l_1 and l_2 in Figure 5 can be calculated. From the two measurements l_1 and l_2, the angle θ_2 can be calculated using the cosine rule as

$$l_1^2 = d_s^2 + l_2^2 - 2d_s l_2 \cos(90 - \theta_2) \tag{1}$$

$$\theta_2 = \sin^{-1}\left(\frac{d_s^2 + l_2^2 - l_1^2}{2d_s l_2}\right) \tag{2}$$

where d_s is d_1+d_2. Then, the distance l_s can be calculated using the cosine rule and x_s can be obtained from l_s as

$$l_s^2 = d_2^2 + l_2^2 - 2d_2 l_2 \cos(90 - \theta_2) \tag{3}$$

$$x_s = l_s / 2 \tag{4}$$

Using the cosine rule one more time, the estimated angle of object's surface can be calculated as

$$\theta_s = \sin^{-1}\left(\frac{l_2^2 - d_2^2 - l_s^2}{2d_2 l_s}\right) \tag{5}$$

It is worth mentioning that this system can provide not only angular information but also more robust performance. Since this system has two receivers, abnormal range measurement data can be detected by comparing the two measurements.

2.3 RIGHT TURNING CAR DETECTION AND WARNING DECISION

In addition to the relative lateral distance and relative angle, relative lateral velocity and relative angular velocity between the car and bicycle can be considered since the velocities involve not only present but also future information. A Kalman filter is used to estimate the relative lateral and angular velocity. The state vector to be estimated is

$$X_s = \{x_s \quad \dot{x}_s \quad \theta_s \quad \dot{\theta}_s\} \tag{6}$$

where x_s is relative lateral distance, $\dot{x}_s$ is relative lateral velocity, θ_s is relative angle, and $\dot{\theta}_s$ is relative angular velocity. The discrete-time model can be modeled as

$$X_s(k+1) = FX_s(k) + w_s(k)\,,\ Z(k) = HX_s(k) + n(k) \tag{7}$$

$$F = \begin{bmatrix} 1 & \Delta t & 0 & 0 \\ 0 & 1 & 0 & 0 \\ 0 & 0 & 1 & \Delta t \\ 0 & 0 & 0 & 1 \end{bmatrix}, H = \begin{bmatrix} 1 & 0 & 0 & 0 \\ 0 & 0 & 1 & 0 \end{bmatrix} \tag{8}$$

where $w_s(k)$ and $n(k)$ are process and measurement noises. While a Kalman filter is used as the estimator, the Mahalanobis distance is also used to reject outliers.

Figure 6 and 7 show experimental data for the two cases, one in which the car is just passing by the bicycle and one in which the car makes a right turn towards the bicycle. As discussed earlier, initial behavior of the lateral distance and velocity of the car are similar in the two cases. Also, the evolution of the relative angle and velocity for the passing car case can be seen in Figure 6. Even though there is ambiguity, the magnitude of velocities from the car passing by the bicycle will be smaller than the other case if the car is passing by the bicycle slowly. Most importantly, if the relative angular velocity compared to relative lateral velocity is checked, we can clearly see the different behavior of the velocities. When the car is turning towards the bicycle, both the angular and lateral velocity change rapidly as the car gets closer. When the car is passing by the bicycle, the change of the angular velocity is initially similar to when the car is turning. However, since the car becomes far from the bicycle, the lateral velocity evolves in the opposite direction, in contrast to the velocity from the turning car. From this physical evidence, two thresholds can be simply and reliably setup for the velocities. If the velocities satisfy both conditions, the turning maneuver can be confirmed properly within a short time.

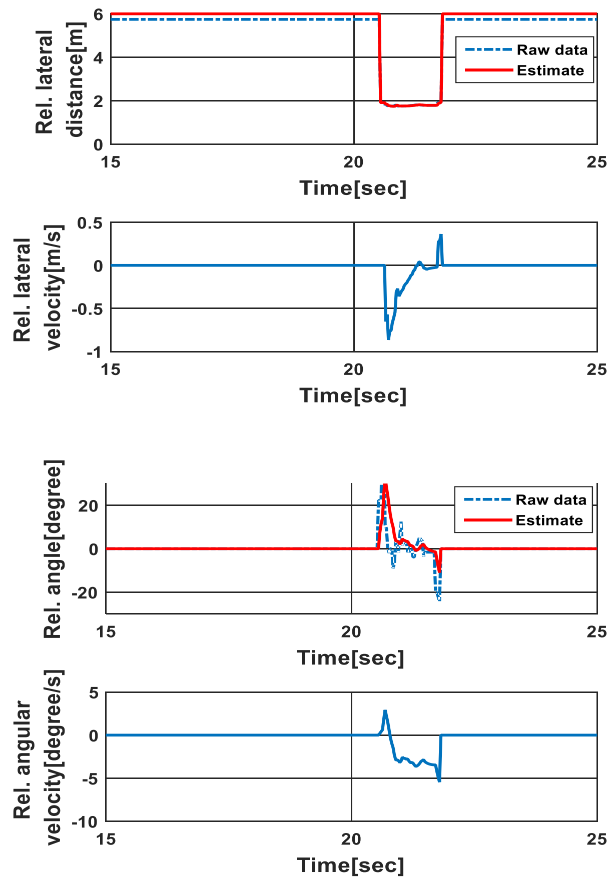

Figure 6. Experimental result when the car is passing by the bicycle.

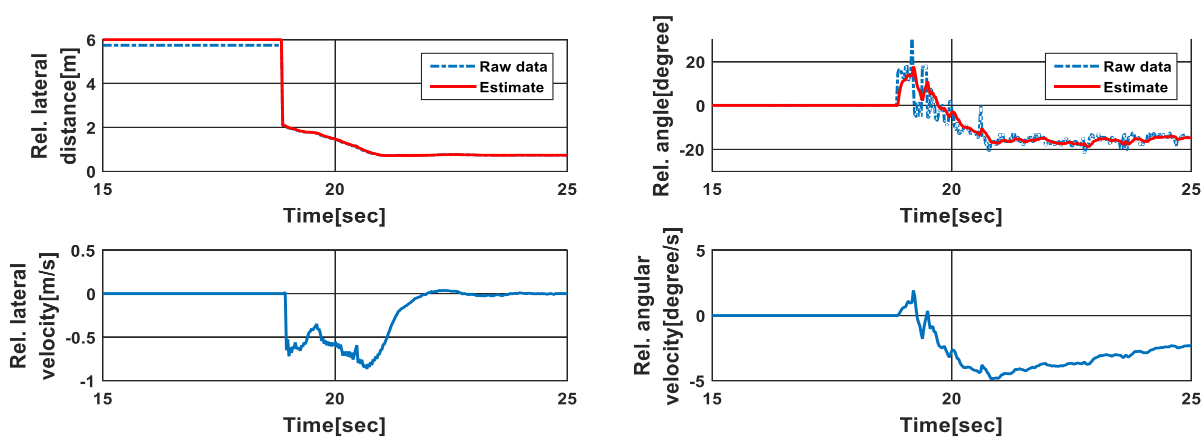

Figure 7. Experimental result when the car is turning into the bicycle.

2.4 REAR COLLISION PREVENTION

In order to address rear collisions, we aim to develop a general target detection and tracking system which can track a rear vehicle that might be right behind the bicycle, or in an adjacent lane next to a bicycle lane, and might be traveling straight or turning in either direction. Figure 8 shows four types of scenarios that are commonly encountered with respect to rear vehicles and bicycles. Due to high cost, size and weight constraints on a bicycle, a low cost laser sensor and a rotating platform are proposed as shown in Figure 9. The laser sensor has a long range (35 meters), small size, weight and low cost ($89, single unit retail) [19]. However, the sensor has only a single laser beam and low sampling frequency (50Hz). This poses the following challenges: First, since the target (vehicle) size is much larger than the spread of the laser beam (~8 milli-radians), the measurement of the laser sensor will not provide adequate spatial information of the target such as lateral and longitudinal position and orientation. For example, unless the measurement is obtained exactly from a corner of the vehicle, either longitudinal or lateral distance between the vehicle and sensor is uncertain. Second, many researchers estimate the target kinematics such as position, orientation and velocity based on measurements from a full scan set (or multiple scans) of an area of interest on the vehicle using expensive LIDARs [5]. However, a complete scan over the full area of interest takes too much time using the proposed laser sensor system due to its low sampling frequency. Due to the above reasons, active sensing which uses an intelligent algorithm for determining real-time laser sensor orientation is necessary to track the target effectively. Here it should be noted that as the rear vehicle's lateral and longitudinal positions change, a *varying* laser sensor orientation is required in real-time to track the vehicle, as shown in Figure 10.

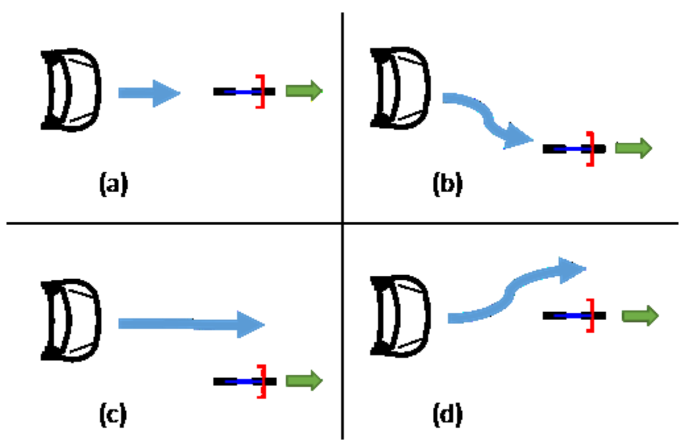

Figure 8. Four types of scenarios of rear approaching vehicle. (a) Approaching right behind, (b) Changing lane to the right, (c) Passing by and (d) Changing lane to the left.

Figure 9. Laser sensor system on bicycle. (a) Rear-facing sensor. (b) Zoomed in.

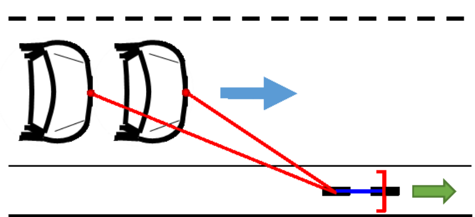

Figure 10. Necessity of changing sensor orientation for tracking.

The rest of this report is organized as follows. In the next section, a clustering based detection algorithm for identifying a target as an on-road vehicle and its experimental performance are presented. Then in Section V, a 1-D vehicle motion tracking system is provided and its experimental performance is discussed. In Section VI, a receding horizon optimization technique for active control and an Interacting Multiple Model (IMM) framework for estimation used for 2-D vehicle motion tracking is discussed and its performance studied in simulations and experiments. Conclusions are presented in Section VIII.

CHAPTER 3: DETECTION OF A REAR APPROACHING VEHICLE

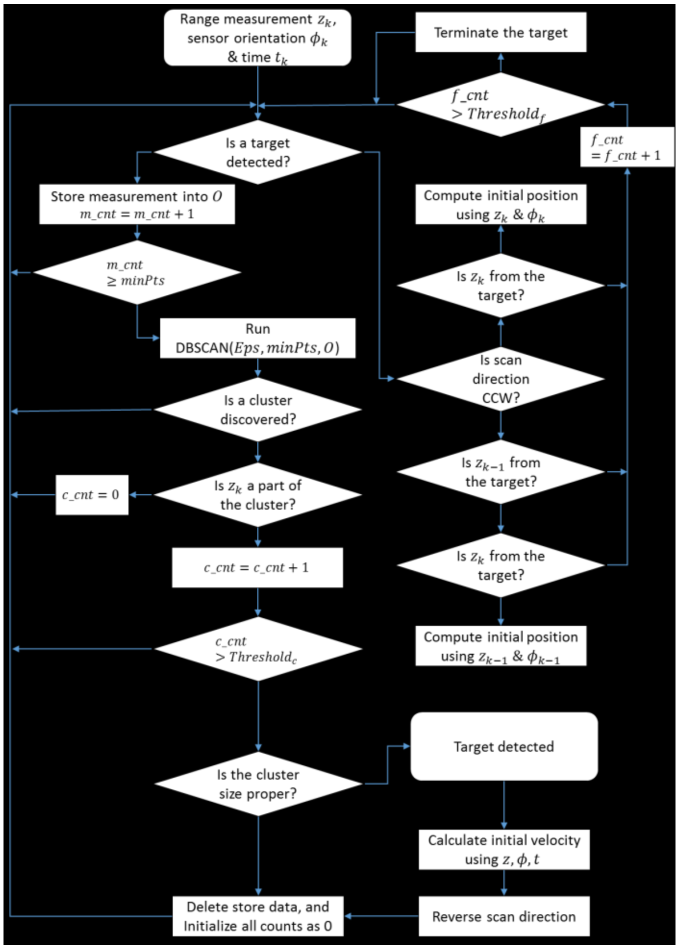

Figure 11. Flowchart of the proposed target detection algorithm with computing the initial conditions of target position and velocity

Detection of a target as a rear approaching vehicle is non-trivial since not only the target vehicle but also the ground and any other objects in the area of interest can be detected by the laser sensor and can initiate tracking. A clustering-based target detection algorithm which also computes the initial conditions of the target's position and velocity is proposed. The flowchart of the proposed algorithm procedure is shown in Figure 11. The Density Based Spatial Clustering of Application with Noise (DBSCAN) [20] is utilized in this algorithm and customized for the bicycle application. The DBSCAN requires two parameters: a minimum radius *Eps* and a minimum number of points within the radius *minPts*. Using these parameters, the DBSCAN can identify clusters by examining the local density of data in spatial data sets. The laser sensor system initially keeps scanning over a pre-determined range and stores measurements to an array. Once a number of stored measurement data exceeds *minPts*, the

DBSCAN examines the data to decide whether it constitutes a cluster or not. By setting proper *Eps* and *minPts*, measurements from small objects or outliers cannot contribute to the cluster. This procedure is iterated until a cluster is discovered and then a certain number of iterations until other points do not contribute to the cluster. After the isolated cluster is found, the cluster is examined by its lateral size. If the size is within thresholds, the cluster is confirmed as a target vehicle. Otherwise, stored data are deleted and this procedure is repeated.

Figure 12 (a) shows the raw experimental data for a rear passing vehicle. The laser sensor system is fixed on a tripod and initially scans open-loop with a 30 degrees fixed range. A vehicle approaches in a straight motion and passes by the sensor system. The measurements are represented on a 2-D map (longitudinal versus lateral distance) using range and orientation of the sensor measurements. Figure 12 (b) shows the result using the proposed clustering method. The outliers (small number of data in isolation) and ground detection points (sparse data) are eliminated.

After the cluster is confirmed as a target, initial conditions of the target kinematics are computed for better tracking performance. An initial relative velocity is calculated using stored data on the center of the vehicle. For instance, most recent data are used when the sensor system detects a target with clockwise direction scan. To the next step, the scan direction is reversed to find initial relative position (right front corner position) of the vehicle. If the reversed scan direction is counter-clockwise (CCW), the sensor system scans over the target until the sensor misses the target. Then, the last measurement before the sensor misses the target is used as initial relative position of the target. If the reversed scan direction is clockwise (CW), the sensor system scans until the sensor obtains first measurement from the target and the measurement is used as the initial relative position of the target. Finally, the target detection is completed, and target motion tracking and estimation start using the calculated initial conditions.

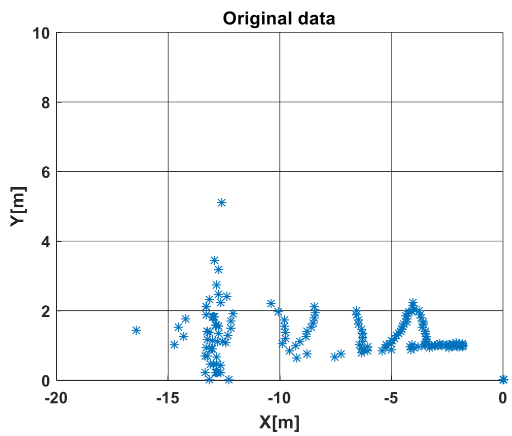

(a)

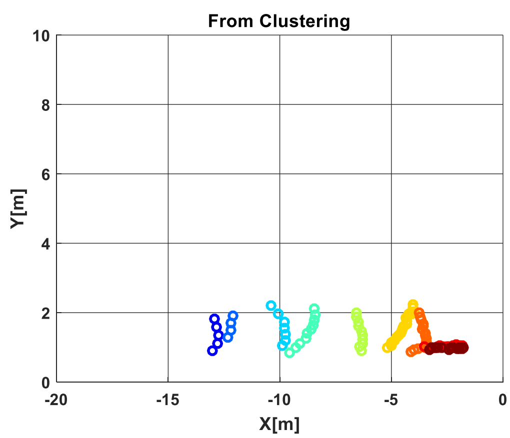

(b)

Figure 12. Results of real laser scans using 30 degrees fixed range. (a) Raw data. (b) Result using the clustering method (colors present each scans). The *Eps* and *minPts* are used as 0.5 m and 4 respectively.

CHAPTER 4: TRACKING OF ONE-DIMENSIONAL VEHICLE MOTION

To begin with, we assume that the vehicle has only 1-D motion. The vehicle could be in the same lane as the bicycle, or in the adjacent lane to the left, if the bicycle is driving in a bicycle lane or a shoulder as shown in Figure 8 (a) and (c). A complete scan over the full area of interest takes too much time for even 1-D vehicle motion tracking using the proposed laser sensor system due to its low sampling frequency. Thus, an efficient control algorithm is needed to control and focus the orientation of the laser sensor in real-time. In this paper, we approximate the geometric shape of the vehicle by a rectangular shape and all variables are defined based on a 2-D coordinate frame attached to the bicycle as illustrated in Figure 13, where ϕ and d are the sensor orientation and range measurement, and x and y are relative longitudinal and lateral distances.

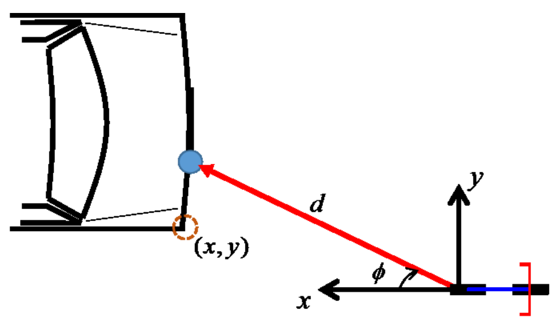

Figure 13. Illustration of 2-D coordinates relative to the bicycle and associated variables.

4.1 RECEDING HORIZON CONTROL FOR 1-D MOTION TRACKING

We first consider the case where the vehicle behind the bicycle is traveling straight without turns. In this case, once the target vehicle is detected, the system focuses on estimation of longitudinal distance between the vehicle and the bicycle. Thus, the sensor system needs to aim at the front of the vehicle continuously to estimate the longitudinal distance. We address this problem using the Model Predictive Control (MPC) approach so as to control the laser sensor to track a reference point on the front of the target vehicle using limited rotational angle changes. The sensor system dynamics are

$$\phi_{k+1} = \phi_k + u_k \tag{9}$$

where u_k is sensor orientation control input at time k. It is too difficult to predict the motion of the target vehicle accurately over multiple time steps due to unknown desired acceleration actions. Therefore, we focus on one step prediction of the motion of the target vehicle to examine sensor orientation control. During 1-D motion, the lateral distance between a point at the front of a target vehicle and bicycle is not changing. Therefore, we can calculate the reference point for sensor tracking using a point at the front of the target vehicle and predicted longitudinal vehicle motion during each time sample. The following optimization problem can be considered:

$$\begin{aligned} &\min_{u_k} \left\| \frac{y_{ref}}{\hat{x}_{k+1}} - \tan(\phi_k + u_k) \right\|^2 \\ &\text{subject to} \quad \hat{x}_{k+1} = f_{1,k}(X_k), \hat{x}_{k+1} > 0 \\ &\qquad\qquad\quad u_k \in U, \phi_{\min} \le \phi_k + u_k \le \phi_{\max} \end{aligned} \tag{10}$$

where y_{ref} can be obtained by calculating the center location of the cluster obtained at the time of the target vehicle detection, X is state vector for the target motion, $f_1(\cdot)$ is the target motion model which corresponds to x, and U is a finite set of feasible control inputs. The control input for the sensor orientation can be obtained by solving the above optimization problem. Practically, the sensor orientation will be less than 90 degrees and larger than -90 degrees in order to scan the area of interest. First, the optimal solution of the optimization problem without control input constraints is found where the derivative is zero. Then, the control input which is closest in value is selected from within the finite set of feasible control inputs.

Preliminary results were presented earlier by us for just the 1-D case in a conference publication [21].

4.2 1-D VEHICLE MOTION ESTIMATION

A Kalman filter is used to estimate the longitudinal vehicle motion. The state vector to be estimated is

$$X = [x \quad v_x \quad a_x]^T \tag{11}$$

where x, v_x, and a_x are relative longitudinal distance, velocity and acceleration. The longitudinal vehicle motion dynamics can be defined as

$$X_{k+1} = \begin{bmatrix} 1 & T & T^2/2 \\ 0 & 1 & T \\ 0 & 0 & 1 \end{bmatrix} X_k + w_k \tag{12}$$

where T is the sampling interval and w is process noise. Since the range and sensor orientation measurements from the laser sensor system have relatively small noise, we compute an equivalent measurement in Cartesian coordinates from the true laser sensor measurement in polar coordinates:

$$z_k = d_k \cos\phi_k \tag{13}$$

This sensor measurement is examined by comparing recent longitudinal distance estimates of the target vehicle. If the measurement is verified to come from the target vehicle, the states are estimated using the Kalman filter with the measurement. Otherwise, the states are estimated by only time updates. After the estimation, the time update using (12) without considering process noise is conducted to predict the longitudinal vehicle motion $\hat{x}_{k+1}$. The predicted longitudinal distance will be used in (10) to obtain the control input.

4.3 SIMULATION RESULTS OF 1-D VEHICLE MOTION

We first implemented the detection algorithm and the 1-D motion tracking algorithm into Matlab so that our algorithm could be verified under various simulated vehicle velocities and accelerations. The simulation environment is constructed using the dimensions of a bicycle and a vehicle based on a 28" wheel bicycle and a midsize sedan. Then, the motion of the bicycle and the vehicle can be expressed by using a linear motion model [22]. It is worth mentioning that the simulation takes into account the incidence angle of a laser beam to objects. The 70 degrees maximum which is obtained from experiments is used as a threshold for maximum incidence angle. Random measurement noise ~$N(0,2^2[\text{cm}])$ is added to this simulation.

A typical situation is simulated in which the bicycle is riding straight and the vehicle is going on the adjacent lane next to the bicycle lane as described in Fig 8 (c). The bicycle is moving with a constant speed of 4.5m/s. The detection is conducted when the target vehicle is within 25m from the sensor. Two parameters *Eps* and *minPts* of DBSCAN set as 0.5m and 4. The finite set of control inputs is {-1, 0, 1} in degrees, and ϕ_{min} and ϕ_{max} are -5 and 90 in degrees respectively.

Figure 14 shows the simulation results using an open-loop fixed scan range (30 degrees). The location of the sensor is marked with a red triangle on the plot. It is clear that the measurements are not available most of the time and estimate updates are slow. Due to the sparse measurement data, the tracking performance is poor. The results of the laser sensor motion control using the receding horizon control method are shown in Figure 15. The tracking performance is significantly better and the estimates are updated very fast by obtaining measurements almost continuously.

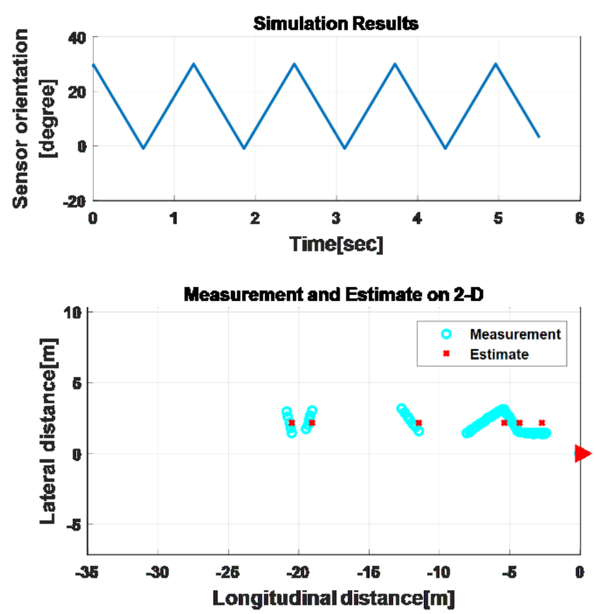

Figure 14. Simulation results using fixed range scans.

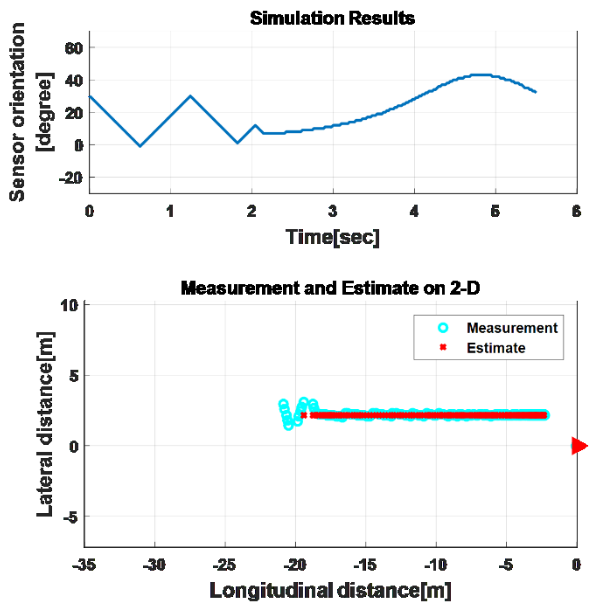

Figure 15. Simulation results using the proposed 1-D motion tracking method.

4.4 EXPERIMENTAL RESULTS OF 1-D VEHICLE MOTION

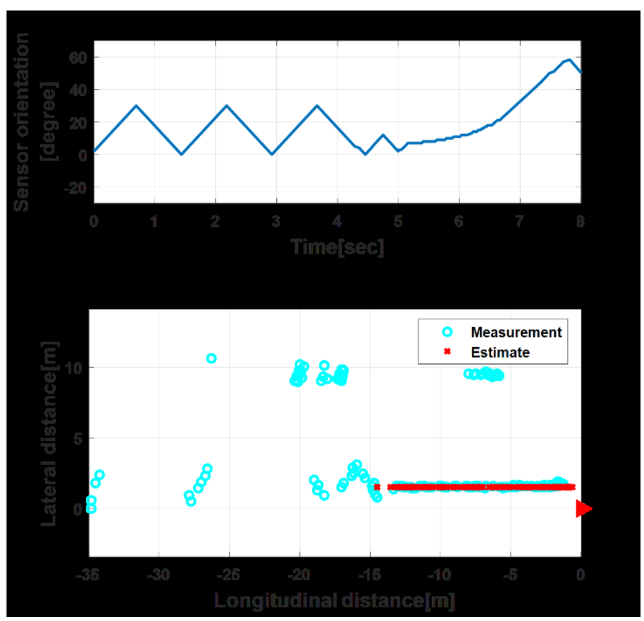

Figure 16. Experimental results using the proposed 1-D motion tracking method.

We conduct experiments involving 1-D vehicle motion in which a vehicle is passing by a bicycle without turns. In order to verify the proposed control and estimation method, a tripod is used to station the laser sensor system on a rotating platform and the lateral distance between the sensor system and the passing vehicle is approximately 2m. An Arduino Mega microcontroller is utilized to implement the proposed detection algorithm and the 1-D vehicle motion tracking methods. The results are well-matched with simulation results and show that the sensor system can track the vehicle position very well as shown in Figure 16.

CHAPTER 5: TRACKING OF TWO-DIMENSIONAL VEHICLE MOTION

In this section, we aim to develop and demonstrate a more general target tracking system which can track both a rear approaching vehicle that might be right behind the bicycle, or a rear vehicle in an adjacent lane next to a bicycle lane, and might be either traveling straight or turning in either direction. Figure 8 shows four types of scenarios that are commonly encountered with respect to rear vehicles and bicycles. We expand the idea of 1-D motion tracking to 2-D motion tracking to track the right front corner of a target vehicle. Like 1-D motion tracking, a desired orientation for the laser sensor system is determined at every sampling time instead of waiting for the end of an open-loop scan range. From this data, despite using a single beam laser sensor with low sampling frequency, not only acquisition of both lateral and longitudinal information but also more robust tracking rather than using small area scanning can be accomplished. We develop a receding horizon controller with an interacting multiple model estimation framework.

Preliminary results of 2-D case were presented earlier by us in a conference publication [23].

5.1 RECEDING HORIZON CONTROL FOR 2-D MOTION TRACKING

For 2-D vehicle motion tracking, we aim to track the right front corner of a target vehicle by measuring alternately distances to the front and side of the vehicle at points close to the right front corner, since tracking this corner provides both lateral and longitudinal distance information. Therefore, the reference point for orientation control needs to be changed depending on the corresponding selection of which information (longitudinal or lateral) is needed. The following optimization problem is therefore constructed for orientation control:

$$u_k^* = \begin{cases} \arg\min\limits_{u_k} \left\| \dfrac{\hat{y}_{k+1} + \delta_y}{\hat{x}_{k+1}} - \tan(\phi_k + u_k) \right\|^2, \\ \text{if longitudinal distance is desired} \\ \arg\min\limits_{u_k} \left\| \dfrac{\hat{y}_{k+1}}{\hat{x}_{k+1} + \delta_x} - \tan(\phi_k + u_k) \right\|^2, \\ \text{if lateral distance is desired} \end{cases} \tag{14}$$

$$\begin{aligned} \text{subject to} \quad & \hat{x}_{k+1} = f_{1,k}(X_k),\ \hat{y}_{k+1} = f_{2,k}(X_k), \\ & \hat{x}_{k+1} > 0 \\ & u_k \in U,\ \phi_{\min} \le \phi_k + u_k \le \phi_{\max} \end{aligned}$$

where $f_2(\cdot)$ is the target motion model which corresponds to y, and δ_x and δ_y are certain distance margins which are used to construct reference points on the target vehicle. The margins need to be small enough for fast measurement updates and to be large enough for robustness to deal with vehicle maneuver changes. Once the vehicle is passing next to the bicycle (i.e., $\hat{x}_{k+1} \le 0$), the sensor system focuses on measuring the lateral distance since it is not possible and not useful to obtain the longitudinal distance.

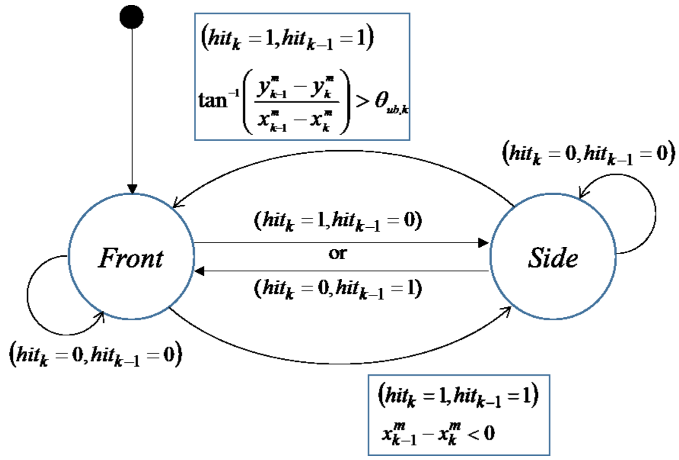

Figure 17. State diagram for determination of reflection location on a vehicle.

It is ideal to obtain the longitudinal distance and lateral distance alternately to deal with vehicle maneuver changes. As soon as obtained information is verified (determination of whether the reflected beam is from the front or side of the vehicle), the reference point needs to be switched to seek the other information. However, it is difficult to determine the location (front or side) of the reflection using only one measurement. Also, every reflection from side or front of the vehicle is not always detectable. For instance, when the target vehicle is far from the sensor, the sensor cannot obtain reflections from the side due to the geometry, i.e., the incidence angle is too large to reflect enough intensity of the beam to the sensor. Similarly, when the target vehicle is very close to the sensor with significant lateral distance (passing vehicle), the sensor cannot obtain reflections from the front. In order to account for these different situations, a finite state machine is utilized with two states: a *Front* state and a *Side* state as shown in Figure 17. The state transitions occur based on the examination of current and previous range measurements d_k and d_{k-1}. For notational simplicity, we define hit_k as an indicator on whether the measurement is from the target vehicle or not at time *k* in Figure 17.

$$hit_k = \begin{cases} 1, & \text{if measurment is from the target vehicle} \\ 0, & \text{otherwise} \end{cases} \tag{15}$$

As discussed before, the initial state starts from the *Front*. In case of not having any measurements from the target vehicle at both current and previous time, we assume that the state remains the same. When the measurement can be obtained at only one of either current or previous samples, a transition from the current state to the other state occurs. If the sensor system acquires two measurements in a row, the decision differs based on the value of the current state. A transition from *Front* to *Side* occurs when the subtraction between the projections of the range measurement to longitudinal axis x_k^m at previous and current time is negative, i.e., $x_{k-1}^m - x_k^m < 0$. Otherwise, the state machine remains at the current state, *Front*. When the current state is *Side*, it remains same if the slope from two measurements corresponds with the orientation of the vehicle. Otherwise, a transition from *Side* to *Front* occurs. Practically, the measurements contain noise and the orientation of the car is hard to estimate accurately using the single beam laser sensor system. Instead of using the strict rule above, we use upper bound for the orientation of the vehicle. The revised condition for the transition from *Side* to *Front* is the following:

$$\tan^{-1}\left(\frac{y_{k-1}^{m}-y_{k}^{m}}{x_{k-1}^{m}-x_{k}^{m}}\right)>\theta_{ub,k} \tag{16}$$

where y_k^m is the projection of the range measurement to lateral axis at time *k*. The upper bound threshold $\vartheta_{ub,k}$ that accounts for passing and left turning car maneuvers is obtained using the estimate of the vehicle orientation and an error margin.

$$\theta_{ub,k}=\hat{\theta}_{k}+\theta_{e} \tag{17}$$

5.2 2-D VEHICLE MOTION ESTIMATION

The 2-D motion of a vehicle is very difficult to be described by only one model since it has basically two distinct maneuvers: straight motion and turning motion. Hence, we present the motion of the vehicle using two models (straight motion and turning motion models) rather than using just one model. There are practical algorithms to estimate target kinematics using this multiple model approach such as generalized pseudo-Bayesian approaches and an interacting multiple model estimation algorithm [24]. In this paper, the Interacting Multiple Model (IMM) algorithm is utilized because the IMM algorithm is considered to be the best compromise between complexity and performance [24].

The IMM system operates multiple filters using the different models in parallel, and computes state estimates using suitable mixing of the estimates and covariance from the two models. The IMM consists of three steps: mixing, mode-matched filtering and combination steps. In the mixing step, the estimates $X_{k-1|k-1}^{j}$ and covariance $P_{k-1|k-1}^{j}$ from each of the filters $(j=1,\ldots,r)$ at the previous iteration are mixed to provide the inputs to each filter. *r* is the number of models utilized. The algorithm of the mixing step is the following:

$$\mu_{i|j,k-1|k-1}=\frac{p_{ij}\mu_{i,k-1}}{\sum_{i=1}^{r}p_{ij}\mu_{i,k-1}},\quad i,j=1,\ldots,r \tag{18}$$

where $\mu_{i|j}$ is called mixing probabilities and p_{ij} is mode transition probabilities which containing the probability of transitioning from mode *i* to *j*. Then initial inputs are

$$\begin{aligned}\hat{X}_{k-1|k-1}^{0j}&=\sum_{i=1}^{r}\hat{X}_{k-1|k-1}^{i}\mu_{i|j,k-1|k-1},\quad j=1,\ldots,r\\ P_{k-1|k-1}^{0j}&=\sum_{i=1}^{r}\mu_{i|j,k-1|k-1}\{P_{k-1|k-1}^{i}+\\ &\quad[\hat{X}_{k-1|k-1}^{i}-\hat{X}_{k-1|k-1}^{0j}]\\ &\quad[\hat{X}_{k-1|k-1}^{i}-\hat{X}_{k-1|k-1}^{0j}]^{T}\},\quad j=1,\ldots,r\end{aligned} \tag{19}$$

Each of the filters with the inputs are executed in the mode matched filtering step. Also, the likelihood and mode probability update are computed as

$$\Lambda_{j,k} = N(z_k - \hat{z}_k^j, S_k^j), \quad j = 1,\ldots,r$$
$$\mu_{j,k} = \frac{\Lambda_{j,k}\sum_{i=1}^{r} p_{ij}\mu_{i,k-1}}{\sum_{i=1}^{r}\Lambda_{j,k}\sum_{i=1}^{r} p_{ij}\mu_{i,k-1}}, \quad j = 1,\ldots,r \tag{20}$$

where S_k^j is the measurement covariance from each filter. Lastly, the estimates from each filter are combined and finalized in the combination step. The procedure is the following:

$$\hat{X}_{k|k} = \sum_{j=1}^{r} \hat{X}_{k|k}^{j}\mu_{j,k}$$
$$P_{k|k} = \sum_{j=1}^{r} \mu_{j,k}\{P_{k|k}^{j} + [\hat{X}_{k|k}^{j} - \hat{X}_{k|k}] \tag{21}$$
$$[\hat{X}_{k|k}^{j} - \hat{X}_{k|k}]^T\}$$

More details for the theory behind the IMM can be found in [24]. Future vehicle motion can be predicted and computed in the IMM framework. After the estimates are obtained, the mixing step is conducted to calculate the mixed initial conditions for the next iteration using (18) and (19). Then, predictions for each mode are computed using its models as

$$\hat{X}_{k+1|k}^{j} = f^{j}(\hat{X}_{k|k}^{0j}), \quad j = 1,\ldots,r \tag{22}$$

The predictions of vehicle motion in (14) can be obtained from

$$\hat{X}_{k+1|k} = \sum_{j=1}^{r} \hat{X}_{k+1|k}^{j}\mu_{j,k} \tag{23}$$

The Constant Velocity model with Polar velocity (CVP) and the nearly Coordinated Turn model with Polar velocity (CTP) [25] are used in the IMM framework. The state vector is

$$X = [x \;\; y \;\; v \;\; \theta \;\; \omega]^T \tag{24}$$

where *v* is the polar velocity and *ω* is the angular velocity in the sensor body frame. The discrete-time state space equation for the CVP model [25] is given by

$$X_{k+1} = \begin{bmatrix} x + vT\cos(\theta) \\ y + vT\sin(\theta) \\ v \\ \theta \\ 0 \end{bmatrix}_k + w_{v,k} \tag{25}$$

where $w_{v,k}$ is zero mean with covariance as

$$Q_{v,k} = diag\left[\begin{bmatrix} \sigma_{vx}^2 & 0 \\ 0 & \sigma_{vy_1}^2 \end{bmatrix}, T^2\sigma_a^2, \begin{bmatrix} 0 & 0 \\ 0 & 0 \end{bmatrix}\right] \tag{26}$$

The discrete-time state space equation for the CTP model [25] and its process noise covariance matrix are given by

$$X_{k+1} = \begin{bmatrix} x + \frac{2v}{\omega}\left\{\sin\left(\frac{\omega T}{2}\right)\cos\left(\theta + \frac{\omega T}{2}\right)\right\} \\ y + \frac{2v}{\omega}\left\{\sin\left(\frac{\omega T}{2}\right)\sin\left(\theta + \frac{\omega T}{2}\right)\right\} \\ v \\ \theta + \omega T \\ \omega \end{bmatrix}_k + w_{t,k} \tag{27}$$

$$Q_{t,k} = diag\left[\begin{bmatrix} \sigma_{vx}^2 & 0 \\ 0 & \sigma_{vy_2}^2 \end{bmatrix}, T^2\sigma_a^2, \begin{bmatrix} T^3\sigma_\alpha^2/3 & T^2\sigma_\alpha^2/2 \\ T^2\sigma_\alpha^2/2 & T^2\sigma_\alpha^2 \end{bmatrix}\right] \tag{28}$$

Since the state space models above are nonlinear, linearized models are used for the Extended Kalman filter combined with the IMM (IMM-EKF).

As discussed earlier, the measurement often contains only partial information about the corner position. Therefore, a validation step for the measurement is needed to utilize only information which corresponds to the corner position of the vehicle. When the measurement is obtained from the front of the vehicle, the projection of the measurement to longitudinal axis provides correct longitudinal distance. However, the projection to lateral axis does not provide correct lateral distance. In order to keep the correct lateral distance, prediction and modified projection are compared and the minimum value is taken as the correct lateral distance. Then the measurement set can be represented as

$$z_k = \begin{bmatrix} d_k \cos\phi_k \\ \min\left(\hat{y}_{k+1|k}, d_k \sin(\phi_k - u_k)\right) \end{bmatrix} \tag{29}$$

When the measurement is obtained from the side of the vehicle, the projections of the measurement provide correct lateral distance but not longitudinal distance. Similarly, the measurement set can be expressed in this case as

$$z_k = \begin{bmatrix} \min(\hat{x}_{k+1|k}, d_k \cos\phi_k) \\ d_k \sin\phi_k \end{bmatrix} \tag{30}$$

This approach is based on the assumption that the true value is the minimum between the projection and prediction of the measurement. It is possible that this assumption gives rise to a wrong result. For example, when the target vehicle is changing lane to the left and the measurement is obtained only from the front of the vehicle, the assumption is no longer valid and provides wrong vehicle maneuver. In order to overcome this problem, virtual measurements x_{vir} and y_{vir} are introduced as

$$\begin{cases} x_{vir,k} = \hat{y}_{k+1|k} / \tan\phi_k, & \text{if the state is } \textit{Front} \\ y_{vir,k} = \hat{x}_{k+1|k} \tan(\phi_k + u_k), & \text{if the stae is } \textit{Side} \end{cases} \tag{31}$$

When measurements cannot be obtained, we know that there is no target vehicle along the line of the sensor orientation. Meanwhile, the target vehicle is located near the line of the sensor orientation since the sensor scans near the corner position. Using this information, measurement validation can be conducted based on the determination of the reflection location using the finite state machine as shown in Figure 17. If the reflection location is *Front*, the measurement set can be determined as

$$z_k = \begin{bmatrix} \max(x_{vir,k}, \hat{x}_{k+1|k}) \\ \hat{y}_{k+1|k} \end{bmatrix} \quad (32)$$

Similarly, if the reflection location is *Side*, the measurement set can be defined as

$$z_k = \begin{bmatrix} \hat{x}_{k+1|k} \\ \max(y_{vir,k}, \hat{y}_{k+1|k}) \end{bmatrix} \quad (33)$$

Then, a measurement model and its noise covariance matrix are

$$Y_k = \begin{bmatrix} 1 & 0 & 0 & 0 & 0 \\ 0 & 1 & 0 & 0 & 0 \end{bmatrix} X_k + n_k \quad (34)$$

$$R = \begin{bmatrix} \sigma_x^2 & 0 \\ 0 & \sigma_y^2 \end{bmatrix} \quad (35)$$

This method prevents estimates from getting stuck at wrong predictions, allows utilizing a simple linear measurement model and enhances the estimation performance by capturing the vehicle maneuver more quickly.

Table 2. RMSE of Position Estimation

Vehicle maneuver	Longitudinal distance error [m]	Lateral distance error [m]
Approaching right behind	0.018542	0.000001
Changing lane to the left	0.045486	0.076450
Passing by	0.036887	0.049382
Changing lane to the right	0.047562	0.111205

5.3 SIMULATION RESULTS OF 2-D VEHICLE MOTION

In this section, results from simulations using the proposed active sensing algorithm are presented. The simulation environment is built using Matlab as described in Section V *C*.

The four scenarios as shown in Figure 8 are simulated using the proposed active sensing algorithm. The initial velocity of the bicycle and the target vehicle set as 4m/s and 11.2m/s respectively. The detection is conducted when the target vehicle is within 30m from the sensor. A pre-determined scan range for the detection is from -6 to 15 in degrees. Two parameters *Eps* and *minPts* of DBSCAN set as 0.5m and 3. In the tracking stage, the finite set of control inputs is {±1, ±1.5, ±2} in degrees based on the reference points at the front or side of the target vehicle. We use δ_y and δ_x as ±0.1m. The ϕ_{min} and ϕ_{max} are -5 and 90 in degrees respectively. For estimation using IMM, the process and measurement noise parameters are σ_{vx}= 0, σ_{vy_1} = 5, σ_{vy_2} = 7, σ_a = 200, σ_α = 0.8, σ_x = 5 and σ_y =15. Also, we use following mode transition matrix:

$$\begin{bmatrix} 0.99 & 0.01 \\ 0.01 & 0.99 \end{bmatrix} \quad (36)$$

Figure 18 and 19 show the simulation results using the proposed active sensing algorithm. Each simulation results from (a), (b), (c) and (d) in Figure 18 and 19 correspond with the scenarios of (a), (b), (c) and (d) in Figure 8. The location of the sensor is marked with a red triangle on the plots. We can see that the sensor system tracks and obtains measurements near the true position of the corner of the target vehicle. Also, results show that the IMM-EKF provides good estimation performance for all the four scenarios. The root mean squre error (RMSE) of position estimates is shown in Table II. Despite the fact that there are both initial position uncertainty and unknown accelerations, the estimation error is small.

5.4 EXPERIMENTAL RESULTS OF 2-D VEHICLE MOTION

Experiments are conducted in order to verify the performance of the proposed active sensing algorithm in situations corresponding to all the four scenarios of Figure 8, of

i) a vehicle approaching right behind a bicycle,
ii) a rear vehicle with a lateral offset initially going straight and then changing lanes to the right,
iii) a rear vehicle with a lateral offset passing by a bicycle, and
iv) a vehicle right behind a bicycle which then changes lanes to the left from behind the bicycle.

In the experiments for scenario i), the vehicle stops quickly before a collision occurs as shown in Figure 21 (a). The proposed algorithm is implemented on the sensor system shown in Figure 9. A Teensy 3.2 microcontroller is utilized as the processor for implementation of the proposed algorithm. The same parameters and optimization constraints are used as in the simulation. Figure 20 and 21 show the experimental results. From the experimental data, it can be seen that the proposed active sensing algorithm provides good tracking performance in all four scenarios. It is very difficult to obtain true trajectories of the vehicle, so we recorded experimental videos and evaluated the tracking performance by comparisons with the video. Also, we can evaluate the performance of experimental results by comparing with the simulation results. The time evolutions of the sensor orientation and vehicle position estimates are almost identical between the simulation and experimental results for corresponding vehicle maneuvers. As the vehicle is approaching right behind the bicycle, the sensor orientation is controlled to zero degree to track the target vehicle in both simulation and experimental results, as shown in Figure 18 (a), (b), and Figure 20 (a), (b). Similarly, the sensor orientation is eventually controlled to 90 degrees to track the passing vehicles in both simulation and experimental results, as shown in Figure 18 (c), (d), and Figure 20 (c), (d). There are some differences in estimated mode probabilities between the simulation and experimental results because it is difficult in practice for the vehicle and bicycle to travel perfectly straight. Also, the tilting and yawing of the bicycle affect its estimation. However, the results of the estimated mode probabilities show very similar trends at the significant vehicle maneuver changes. The experimental results verify that the sensor system using the proposed active sensing algorithm successfully tracks the target vehicle for all four vehicle scenarios.

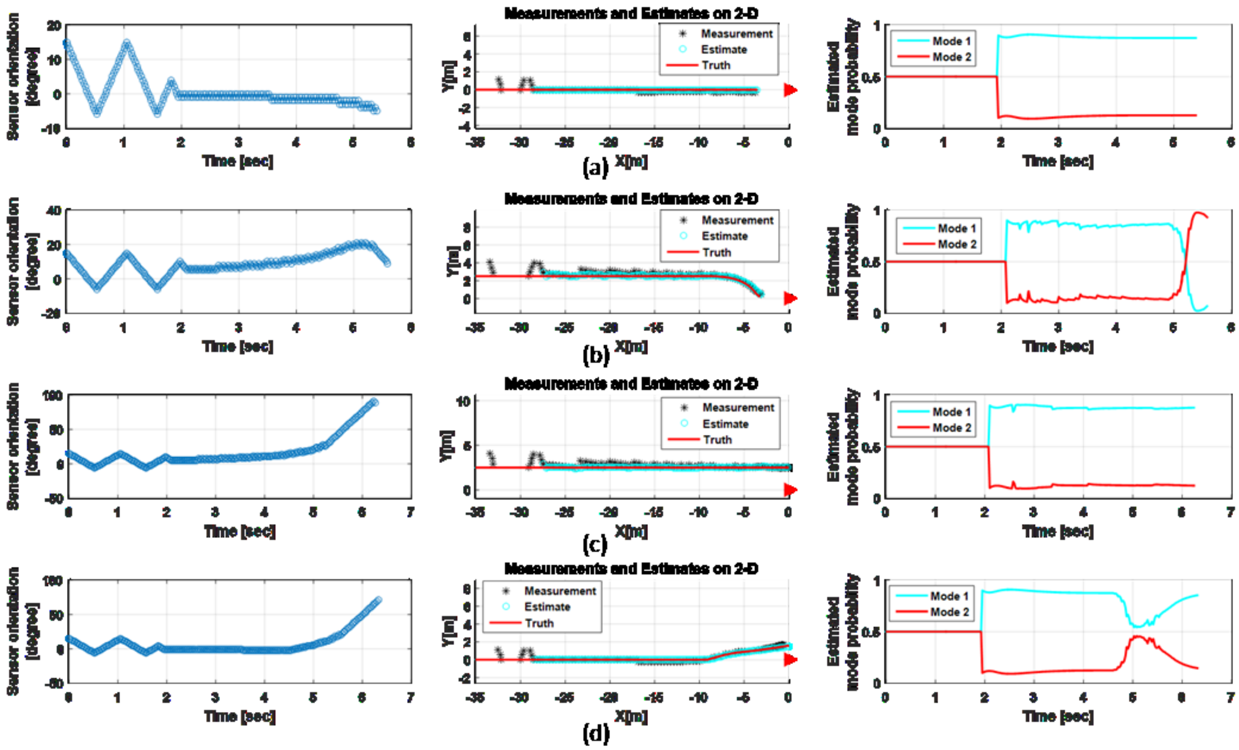

Figure 18. Simulation results of sensor orientation, true trajectories, measurements and estimates on 2-D map, and estimated mode probabilities for target vehicle maneuver corresponding to (a) Approaching right behind, (b) Changing lane to the right, (c) Passing by, and (d) Changing lane to the left.

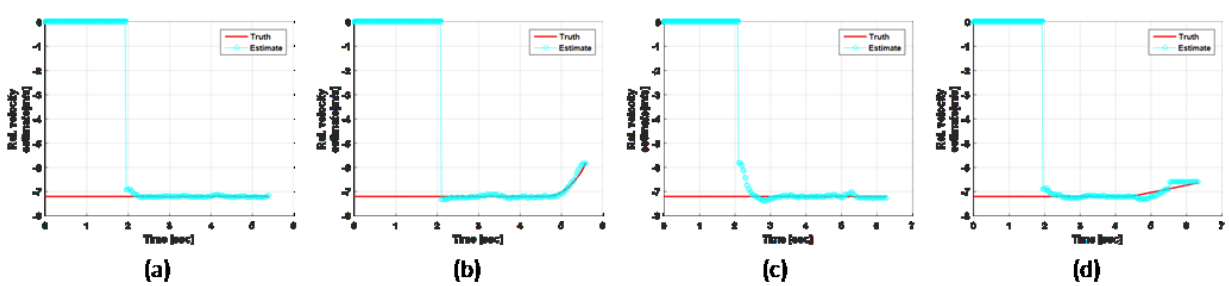

Figure 19. Simulation results of relative velocity estimates for target vehicle maneuver corresponding to (a) Approaching right behind, (b) Changing lane to the right, (c) Passing by, and (d) Changing lane to the left.

In simulations done by this research team, collision from rear vehicles can be prevented safely, even after allowing for a 1 second reaction time of the driver (the driver starts braking 1 second after the alert is sounded) and requiring a 3m safety distance margin (the vehicle stops 3m before the bicycle). The alert is provided to both the driver and bicyclist when the time to collision between the vehicle and bicycle is less than 1.85 seconds. As long as the maximum allowable relative velocity is 11.9 m/s and the range of the laser sensor is 25m, the rear collision can be prevented. This maximum relative velocity might be adequate for an urban road, but higher relative velocities could be encountered on a rural road. Unfortunately, the only way to allow for higher relative velocities is to incorporate sensors with larger range measurement.

Once a vehicle has been detected, the developed vehicle tracking system was found to work successfully for continuous tracking of the vehicle's lateral and longitudinal positions. However, one situation in which the tracked vehicle can be lost is during significant yaw and tilt motion of the bicycle. Normal tilt and yaw during riding on a straight road was not a concern, except that it could reduce the working range of the laser sensor from 35m to 20m.

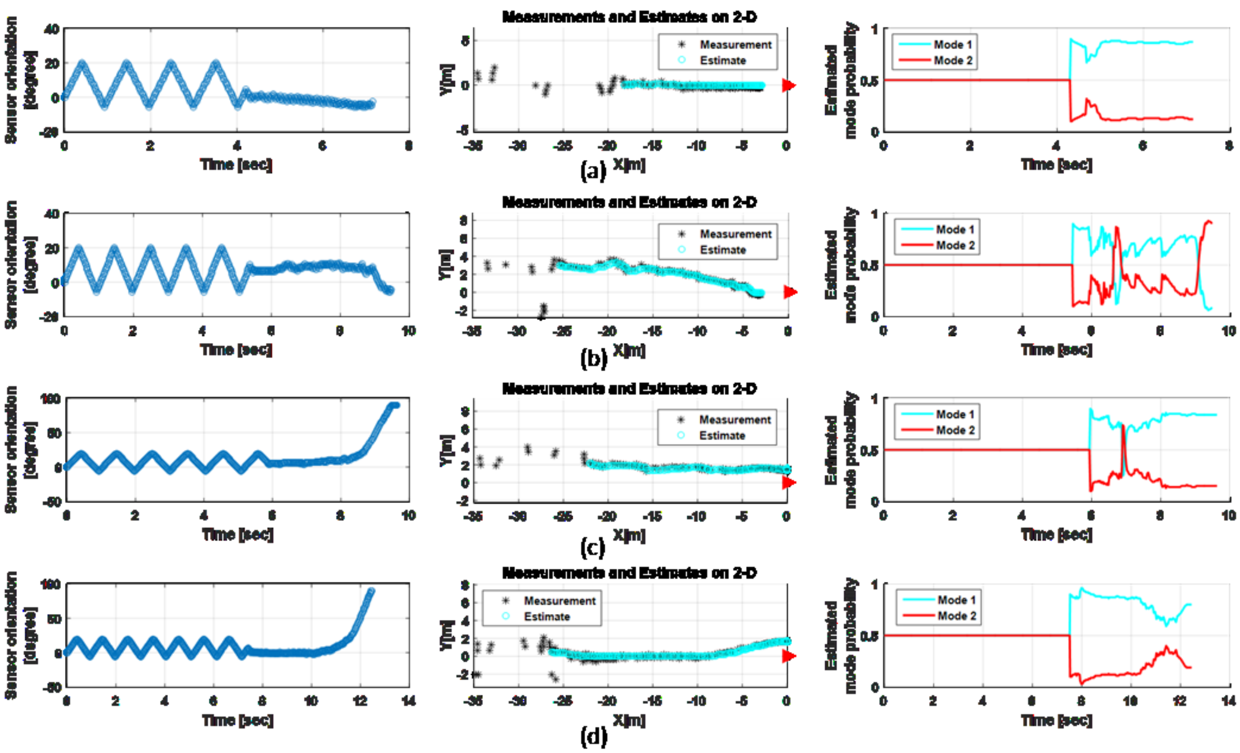

Figure 20. Experimental results of sensor orientation, measurements and estimates on 2-D map, and estimated mode probabilities for target vehicle maneuver corresponding to (a) Approaching right behind, (b) Changing lane to the right, (c) Passing by, and (d) Changing lane to the left.

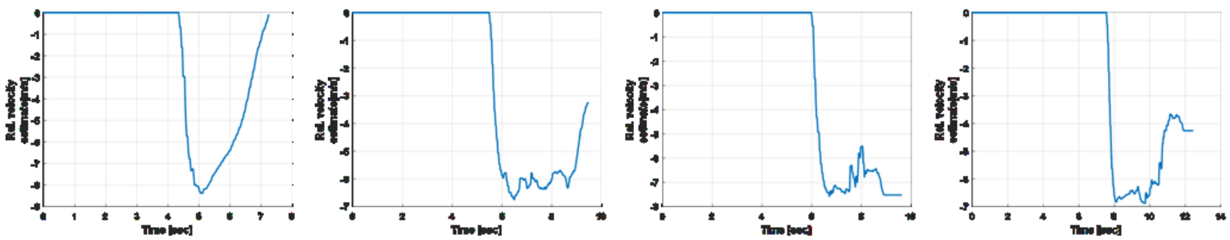

(a) (b) (c) (d)

Figure 21. Experimental results of relative velocity estimates for target vehicle maneuver corresponding (a) Approaching right behind, (b) Changing lane to the right, (c) Passing by, and (d) Changing lane to the left.

CHAPTER 6: EVALUATION OF REAR COLLISION PREVENTION SYSTEM ON REAL WORLD ROADS

The rear collision prevention system has been tested multiple times on real world roads. The tests were conducted on urban roads near the University of Minnesota and have involved many miles of riding. From the tests, it has been confirmed that the developed active sensing system shows capability to track vehicles, including in situations involving a continuous series of passing cars of different types and sizes. The laser sensor mounted on a rotational platform and a camera are equipped on at the rear of the bicycle, as shown in Figure 22.

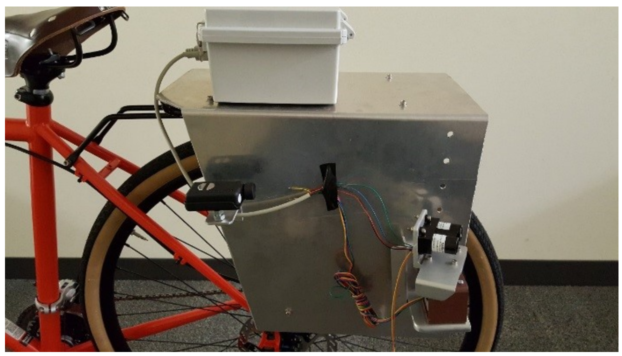

Figure 22. Active sensing system (rotational laser sensor system, micro-controller and battery) and camera on a bicycle

The camera records experimental video in order to help manually analyze the test data from the active sensing system. The most common situation encountered during real world tests is one in which the bicycle is riding in a bicycle lane and a series of cars are driving on the adjacent lane next to the bicycle lane. Figure 23 shows screen shots extracted from one such experimental video. It can be seen that different types of cars are detected and tracked in the test.

(a) Minivan **(b) Sedan**

Figure 23. Screen shots of the experimental video on actual road

For many different types of cars (sedans and SUVs), the developed active sensing system can track the lateral and longitudinal position of the car continuously as the laser sensor automatically controls and focuses on the moving car, as shown in Figure 24.

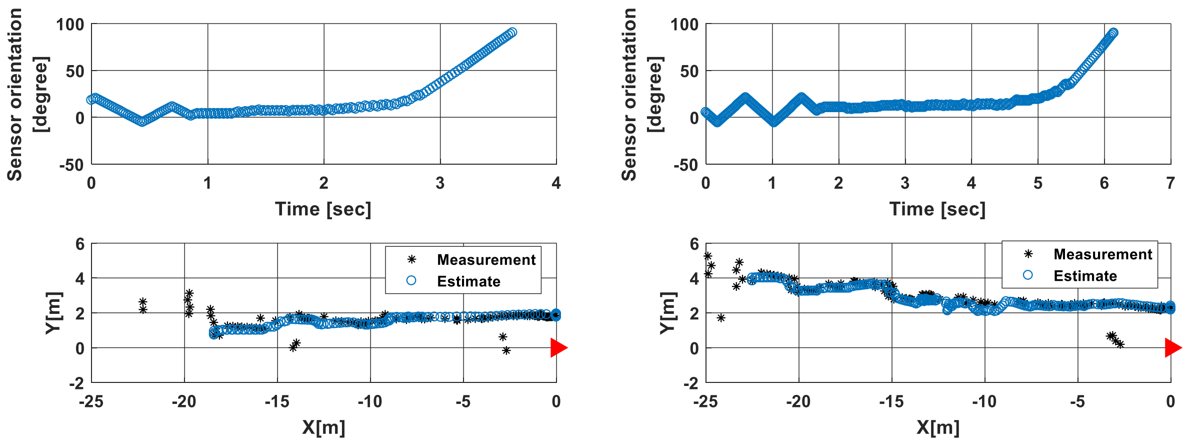

(a) Minivan **(b) Sedan**

Figure 24. Experimental results of sensor orientations, measurements and estimated trajectories on 2-D map

It is also seen that the developed active sensing system can track a series of different cars successfully. After the active sensing system confirms that a car being tracked is safely passing by the bicycle, the system then quickly searches and detects a new target car for tracking, as shown in Figure 25.

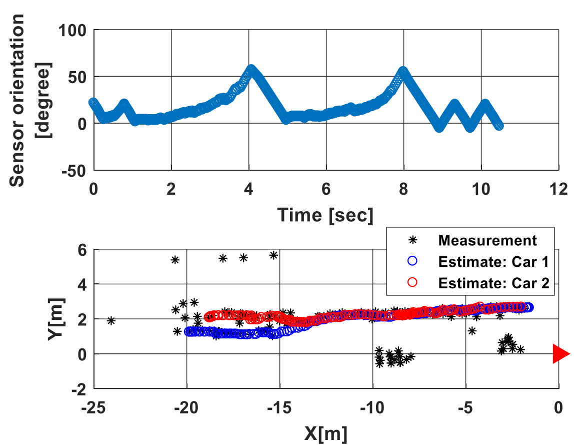

Figure 25. Experimental results (series of two cars) of sensor orientations, measurements and estimated trajectories on 2-D map

Figure 26 shows another experimental result from an actual road test, again in a situation of a series of passing cars. Screen shots of the experimental video show each target vehicle in the situation, as seen in Figure 27.

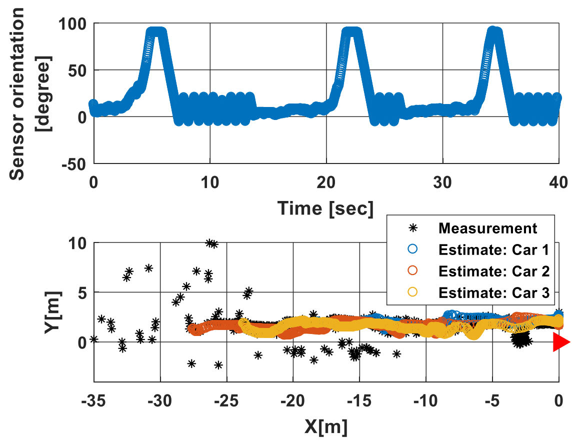

Figure 26. Experimental results (series of three cars) of sensor orientations, measurements and estimated trajectories on 2-D map

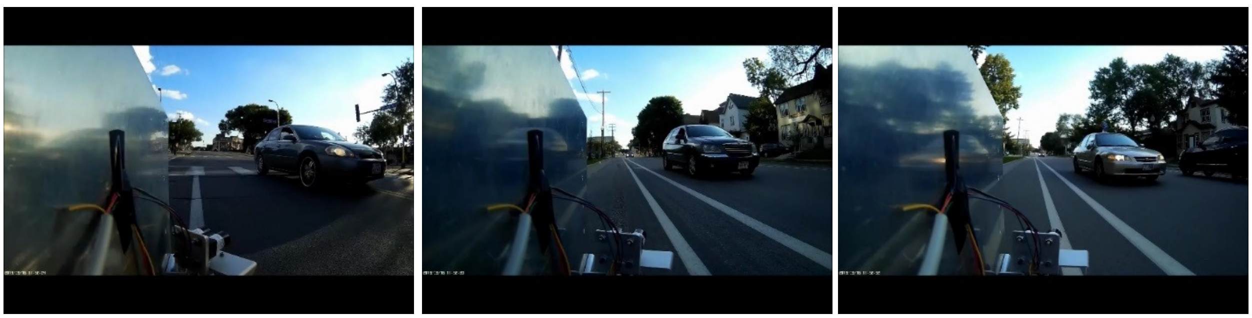

(a) Car 1 (b) Car 2 (c) Car 3

Figure 27. Screen shots of the experimental video on actual road

CHAPTER 7: CONCLUSIONS

Cost, size and power constraints highly limit the type of sensors that can be used on a bicycle for tracking distances to other vehicles on the road. This work proposed a highly inexpensive custom triad sonar sensing system for tracking side vehicles that could potentially turn right and collide with the bicycle. Also, a single-beam laser sensor mounted on a rotationally controlled platform for detection and tracking of rear vehicles was proposed, in order to provide collision warnings to both the motorist and bicyclist. Since the laser sensor could only measure one reflection at a time, the rotational orientation of the laser sensor needed to be controlled in real-time in order to detect and continue to focus on the tracked vehicle, as the vehicle's lateral and longitudinal distances keep changing. This tracking problem requires controlling the real-time angular position of the laser sensor to stay focused on the vehicle, even without knowledge of the vehicle's future trajectory. The challenge is addressed by an active sensing algorithm which uses a novel receding horizon framework for active orientation control and an interacting multiple model framework for vehicle state estimation. The receding horizon controller determines the optimal control input to the sensor based on predicted future vehicle motion under control input constraints. The vehicle motion is predicted in the interacting multiple model framework. The interacting multiple model allows for different types of vehicle maneuvers. Simulation results were presented to show the performance of the developed tracking control system. Extensive experimental results were also presented from an instrumented bicycle to show the performance of the system in detection and tracking of rear vehicles during both straight and turning maneuvers.

CHAPTER 8: FUTURE WORK

One major positive outcome of this project has been obtaining of a research grant funded by the National Science Foundation to carry out follow-on work on the bicycle collision prevention system. In particular, the following major tasks are planned in the NSF project:

a) Development of a collision prevention system for traffic intersections that addresses collisions with left turning vehicles and with cross-traffic

b) Conducting of human factors studies that determine the most effective audio and visual alert systems for efficient human intervention to prevent collisions

c) Conducting a large field operational test consisting of a two-stage 6-month real world operational use cycle involving 10 bicyclists with significant urban commutes. Such a field operational test will more extensively test scenarios that might be rare and might not yet have been anticipated by the authors.

REFERENCES

1) National Highway Traffic Safety Administration (April 2014), “Bicyclists and other cyclists traffic safety facts,” NHTSA, Report. Available: http://www.nhtsa.gov/Bicycles

2) Insurance Institute for Highway Safety (March 2015), “Bicycle crash study could guide design of bicyclist detection system,” IIHS, Report, Volume 50, Number 3..

3) K. McLeod, and L. Murphy (May 2014), “Every bicyclist counts,” League of American Bicyclists, Report.

4) S. Blenski (January 2013), “Understanding bicyclist-motorist crashes in Minneapolis, Minnesota,” City of Minneapolis Public Works Department, Report, Minneapolis, Minnesota.

5) Mukhtar, L. Xia and T. B. Tang (October 2015), "Vehicle detection techniques for collision avoidance systems: A Review," IEEE Transactions on Intelligent Transportation Systems, vol. 16, no. 5, pp. 2318-2338.

6) M. E. Farmer and M. P. Bruce (July 4, 2000), "Predictive collision sensing system," U.S. Patent 6,085,151.

7) G. R. Widmann, M. K. Daniels, L. Hamilton, L. Humm, B. Riley, J. K. Schiffmann, D. E. Schnelker, and W. H. Wishon (2000), “Comparison of lidar-based and radar-based adaptive cruise control systems,” No. 2000-01-0345. SAE Technical Paper.

8) Y. Wei, H. Meng, H. Zhang and X. Wang (2007), "Vehicle Frontal Collision Warning System based on Improved Target Tracking and Threat Assessment," in *2007 IEEE Intelligent Transportation Systems Conference*, Seattle, WA, pp. 167-172.

9) F. Jiménez and J. E. Naranjo (August 2011), "Improving the obstacle detection and identification algorithms of a laserscanner-based collision avoidance system," *Transportation research part C: emerging technologies*, vol. 19, no. 4, pp. 658-672.

10) H. Cho, P. E. Rybski and W. Zhang (2010), "Vision-based bicycle detection and tracking using a deformable part model and an EKF algorithm," in 13th International IEEE Conference on Intelligent Transportation Systems, Funchal, pp. 1875-1880.

11) S. Kamijo, K. Fujimura and Y. Shibayama (2010), "Pedestrian detection algorithm for on-board cameras of multi view angles," in 2010 IEEE Intelligent Vehicles Symposium, San Diego, CA, pp. 973-980.

12) Mobileye. *Mobileye 5 Series* [Online]. Available: http://www.mobileye.com/en-uk/products/mobileye-5-series/

13) Northeastern University. (2014, Jan. 21). Northeastern students develop ‘Smart Bike’ tech to curb cycling death [Online]. Available: http://www.bizjournals.com/boston/blog/startups/2014/01/northeastern-students-develop-smart.html

14) S. B. Eisenman, E. Miluzzo, N. D. Lane, R. A. Peterson, G-S. Ahn, and A. T. Campbell (2007), “The BikeNet mobile sensing system for cyclist experience mapping,” in *5th ACM Conference on Embeded Networked Sensor Systems (SenSys 2007)*, Sydney, Australia, pp. 87 - 101.

15) S. B. Eisenman, E. Miluzzo, N. D. Lane, R. A. Peterson, G-S. Ahn, and A. T. Campbell (December 2009), “BikeNet: A mobile sensing system for cyclist experience mapping,” *ACM Transactions on Sensor Networks (TOSN)*, vol. 6, no. 1.

16) S. Smaldone, C. Tonde, V. K. Ananthanarayanan, A. Elgammal, and L. Iftode (2011), “The cyber-physical bike: a step towards safer green transportation,” In *12th Workshop on Mobile Computing Systems and Applications*, Phoenix, AZ, pp. 56 – 61.

17) Garmin. *Varia Rearview Radar* [Online]. Available: https://buy.garmin.com/en-US/US/p/518151

18) Vanhawks. *Valour* [Online]. Available: https://vanhawks.com/

19) Pulsedlight. *Lidar-lite* [Online]. Available: https://pulsedlight3d.com/

20) M. Ester, H. P. Kriegel, J. Sander, and X. Xu (August 1996), "A density-based algorithm for discovering clusters in large spatial databases with noise," *Kdd*, vol. 96, no. 34, pp. 49-60.

21) W. Jeon and R. Rajamani (2016), “A novel collision avoidance system for bicycles,” in *Proceedings of the* 2016 American Control Conference (ACC), Boston, MA, 2016, pp. 3474-3479.

22) S. Thrun, W. Burgard, and D. Fox (2005), *Probabilistic robotics*. MIT press.

23) W. Jeon and R. Rajamani (2017), “Two-dimensional active sensing system for bicyclist-motorist crash prediction," in *Proceedings of the* 2017 American Control Conference (ACC), Seattle, WA, pp. 2315-2320.

24) Y. Bar-Shalom, X. R. Li, and T. Kirubarajan (2004), *Estimation with applications to tracking and navigation: theory algorithms and software*. John Wiley & Sons.

25) X. Rong Li and V. P. Jilkov (October 2003), "Survey of maneuvering target tracking. Part I. Dynamic models," in *IEEE Transactions on Aerospace and Electronic Systems*, vol. 39, no. 4, pp. 1333-1364.

26) S. Taghvaeeyan and R. Rajamani (February 2014), “Two-Dimensional Sensor System for Automotive Crash Prediction,” *IEEE Transactions on Intelligent Transportation Systems*, Vol. 15, No. 1, pp. 178-190.